Elasticity of mechanical oscillators in nonequilibrium steady states: Experimental, numerical, and theoretical results

Livia Conti,[1] Paolo De Gregorio,[2,3] Michele Bonaldi,[4,5] Antonio Borrielli,[4,5] Michele Crivellari,[6] Gagik Karapetyan,[1] Charles Poli,[1] Enrico Serra,[5,7] Ram-Krishna Thakur,[1] and Lamberto Rondoni[2,3]

[1]*INFN, Sezione di Padova, Via Marzolo 8, I-35131 Padova, Italy*

[2]*Dip. di Matematica, Politecnico di Torino, Corso Duca degli Abruzzi 24, 10129 Torino, Italy*

[3]*INFN, Sezione di Torino, Via P. Giura 1, 10125 Torino, Italy*

[4]*Institute of Materials for Electronics and Magnetism, Nanoscience-Trento-FBK Division, 38123 Povo (Trento), Italy*

[5]*INFN, Gruppo Collegato di Trento, Sezione di Padova, 38123 Povo (Trento), Italy*

[6]*Microtechnology Laboratory, Fondazione Bruno Kessler, 38123 Povo (Trento), Italy*

[7]*Interdisciplinary Laboratory for Computational Science (LISC), FBK-University of Trento, 38123 Povo (Trento), Italy*

(Received 21 March 2012; published 11 June 2012)

We study experimentally, numerically, and theoretically the elastic response of mechanical resonators along which the temperature is not uniform, as a consequence of the onset of steady-state thermal gradients. Two experimental setups and designs are employed, both using low-loss materials. In both cases, we monitor the resonance frequencies of specific modes of vibration, as they vary along with variations of temperatures and of temperature differences. In one case, we consider the first longitudinal mode of vibration of an aluminum alloy resonator; in the other case, we consider the antisymmetric torsion modes of a silicon resonator. By defining the average temperature as the volume-weighted mean of the temperatures of the respective elastic sections, we find out that the elastic response of an object depends solely on it, regardless of whether a thermal gradient exists and, up to 10% imbalance, regardless of its magnitude. The numerical model employs a chain of anharmonic oscillators, with first- and second-neighbor interactions and temperature profiles satisfying Fourier's Law to a good degree. Its analysis confirms, for the most part, the experimental findings and it is explained theoretically from a statistical mechanics perspective with a loose notion of local equilibrium.

DOI: 10.1103/PhysRevE.85.066605 PACS number(s): 43.40.+s, 62.20.de, 02.70.Ns, 65.40.De

I. INTRODUCTION

An important property of structural materials is their ability to regain the initial shape once a load is removed. This is quantified by the elastic modulus. Hooke's law predicts a linear relationship between stress and strain, as long as the stress remains below a given threshold, called elastic limit, which depends on the material [1]. Given the wide variety of working conditions of products in the real world, it is important to know the elastic modulus as a function of temperature, from the lowest ones up to near the melting point. From a more fundamental perspective, the study of the tunneling states in amorphous and disordered crystalline solids [2,3] has also spread the interest in low temperature elastic properties. Indeed, several studies have appeared in the literature, reporting measurements of the elastic modulus in wide temperature ranges for a large number of materials. Laws to predict the behavior of elasticity versus temperature have been proposed [4], sometimes also with some theoretical justification [5]. Apart from a reduced class of materials, including ferromagnetic ones, these laws describe the observed behavior to a good approximation.

We note that all of the above-mentioned studies refer to materials in thermodynamic equilibrium. On the contrary, structural materials are more often employed in nonequilibrium states, either transient or stationary. Indeed, a number of papers have appeared reporting vibration studies of pieces under thermal gradients (e.g., Refs. [6,7]); this literature is focused on the prediction of the eigenfrequencies for some specific shapes (e.g., rectangular plates), of interest to space technology and mechanical sciences, under the assumption of a temperature field in the specimen and of a known change of the elastic modulus with temperature.

Whether this simple approach is justified is not as obvious as it might appear and is related to the validity of the local equilibrium hypothesis, although such condition should be commonplace for macroscopic objects. To our knowledge there is very little reported in the literature about this issue, and the only experimental study focuses on the frequency changes of a piezoelectric ceramic subject to thermal differences between -40 and $+50$ °C [8]. In this paper we investigate both experimentally and theoretically how the elastic behavior of solids is affected by nonequilibrium steady states associated to temperature differences.

For the experiment we employ resonators of two different materials, a metal, namely an aluminum alloy, and a semiconductor, namely single-crystal silicon; we investigate how the oscillators resonance frequencies change with the temperature from room temperature down to about 200 K, with and without thermal differences across the oscillators up to $\sim$15%. From the theoretical and numerical side we develop a simple model for a solid resonator based on a chain of anharmonic oscillators for which we predict analytically the modulus of elasticity also in the presence of temperature differences at the chain extremes, on the basis of the potential between the chained oscillators. Then we implement molecular dynamics simulations of such a model to compute the modulus of elasticity and compare the numerical results with the theoretical ones. This research is part of a wider scientific effort [9] that focuses on the study of the statistical mechanical properties of low-loss mechanical oscillators subject to

steady-state thermal gradients. Our main concern is the investigation of the spontaneous vibration fluctuations of the nonequilibrium oscillators and how they differ from the Gaussian distribution of the thermal noise predicted at equilibrium by the fluctuation-dissipation theorem [10,11].

Description of the experimental setup is given in Sec. II while the experimental measurements are reported in Sec. III. The theoretical framework for predicting the elastic modulus of our one-dimensional model of a solid resonator is described in Secs. IV A and IV B for the equilibrium and nonequilibrium cases, respectively; the numerical results obtained via molecular dynamics simulations are shown in Sec. IV D. Then in Sec. V we discuss the implications of the results obtained by the two approaches.

II. THE EXPERIMENTAL SETUP

To study the elastic properties in the presence of nonequilibrium states we have developed two mechanical oscillators that we can subject to thermal differences. The oscillator materials are chosen among low-losses ones; in fact, we intend to study the nonequilibrium phenomena in situations similar to those of high-precision experiments, such as gravitational wave detectors, where the thermal noise associated to losses needs to be minimized. One of the oscillators is realized in an aluminum alloy, namely Al5056, which is used in the marine industry and for cable sheathing and wire screens; it meets our purposes since it shows very low mechanical losses at cryogenic temperatures (intrinsic mechanical losses $\lesssim 3 \times 10^{-8}$ below 10 K), a feature that motivates its usage in resonant gravitational wave detectors [12]. The other oscillator is realized in single-crystal silicon. Silicon is the elective material for most microelectromechanical systems(MEMS) [13]; it shows mechanical losses as low as 5×10^{-10} at 3.5 K and 10^{-8} at room temperature. The latter figure is one of the main reasons for choosing silicon as elective material for next-generation gravitational wave detectors [14].

A. The Al5056 oscillator

The Al5056 oscillator is described in Ref. [9] and briefly in the following. It consists of a rod with cross-shaped cross-section, fixed at one end and loaded by a mass (referred to as m_l in the following) at the other end. The rod is kept along the vertical axis with the load mass at the bottom. The first longitudinal mode occurs at $f_o \sim 1.6$ kHz and represents the oscillator we focus on. Figure 1 represents the piece displacement corresponding to the acoustic mode; continuous line shows the shape of the piece at rest. Vibrations of the load mass are measured by a capacitive readout coupled to a low-noise amplifier. The capacitive sensor is realized by facing an aluminum plate to the bottom surface of the load mass; the plate is supported by two arms that extend along the vertical direction at two sides of the rod. The 44-μm-wide capacitor gap is realized by a teflon spacer between the arms and the plate. The capacitive sensor works in a constant charge configuration; measurements reported in this paper were taken after biasing to 5V, corresponding to an electric field of 1.1×10^5 V/m when no thermal differences are applied. The corresponding displacement sensitivity is about 4×10^{-14} m/$\sqrt{Hz}$ around the oscillator resonance; this same capacitor has been biased up to 7.3 MV/m, demonstrating a sensitivity of 6×10^{-16} m/$\sqrt{Hz}$.

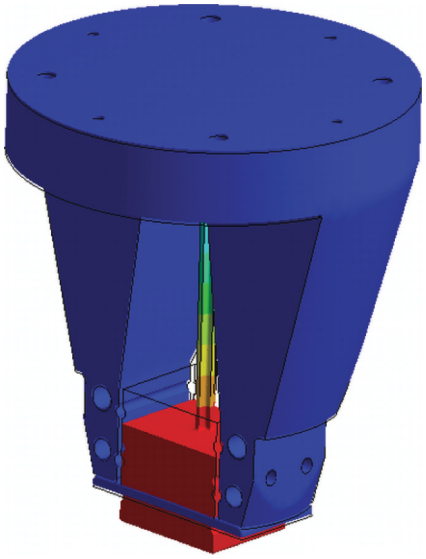

FIG. 1. (Color online) Maximum deformation of the oscillator when vibrating at the first longitudinal mode, which resonates at about 1.6 kHz with a quality factor of about 10^3. The continuous line shows the shape of the body when at rest. The vibration amplitude is shown in color code (online only). The displacement scale has been amplified to better show the displacement; the mechanical interference with the electrode is only apparent.

With a high-stability negative temperature coefficient (NTC) thermistor, we measured the temperature T_1 of the rod top end; the NTC resistance was measured using a four-wire configuration. Using Peltier cells placed on top of the vacuum box, we implemented an active feedback loop, which can stabilize T_1 to a set point just below room temperature, with a residual variation within ± 0.05 K over a period of one month [17]. For the purpose of setting and controlling a temperature difference across the oscillator, we faced the oscillating mass to a thermal source on one side and to a thermopile on the other side, as detailed in Ref. [17]; the thermopile gave a measurement of the oscillating mass temperature T_2.

The oscillator was placed in a vacuum box on top of a three-stage mechanical suspension, which lowers the environmental mechanical noise at the oscillator input by 180 dB [16], thus reducing it to a negligible level. A piezoelectric actuator was placed close to the oscillator and was used to exert a mechanical excitation at its top end.

B. The silicon oscillator

We used a custom-made mechanical oscillator, which we name the quadruple paddle oscillator (QPO), working at audio frequency with low mechanical losses. Our resonator is similar to the double paddle oscillator developed by Spiel *et al.* [18] in the sense that it possesses a number of normal modes with negligible clamping losses because of their good insulation from the support frame; at the same time, it allows us to integrate on one side of its structure a thermal source necessary for the production of a thermal difference along the device.

As shown in Fig. 2, a QPO consists of three inertial units, head and wings, which are connected by a torsion

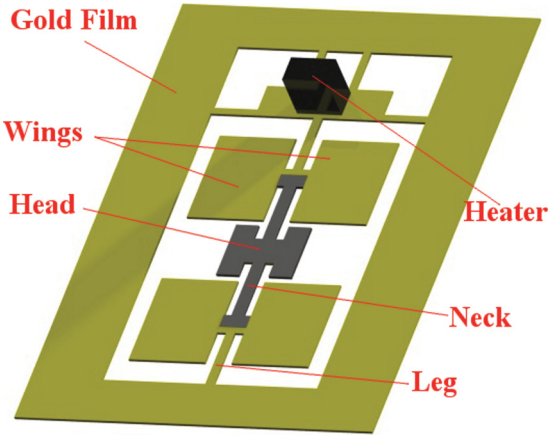

FIG. 2. (Color online) Design of the quadruple paddle oscillator illustrating its different sections. A thin gold layer covers the resonator and provides the electrodes for driving and displacement reading. The head and the neck are not coated to avoid additional dissipation from the metal film.

rod, called neck. Each couple of wings is connected to the supporting structure by another torsion rod, the leg. One leg is connected to the outer frame, the other to an intermediate pad designed to host a heater. This system can be visualized as a coupled oscillator consisting of three masses (head and wings) and of three springs (neck and legs) that twist or bend in different directions, originating several composite vibration modes. Some of these modes, the so-called antisymmetric torsion modes (AS), are of particular interest because of their low internal losses. As shown in Fig. 3 they consist of a twist of the neck around the QPO symmetry axis and a synchronous oscillation of the wings around an axis on the QPO plane and orthogonal to the QPO symmetry axis. The oscillations of head and wings can be in phase (AS1 mode) or out of phase (AS2 mode). For the AS modes the elastic energy is primarily located at the neck, where the maximum strain field occurs during the oscillations, while the leg remains at rest and the frame can be supported by the sample holder with negligible energy dissipation. Another mode that induces a negligible strain in the legs is the wing torsion (WT) mode, where the head remains at rest because the neck is twisted in the opposite direction by the synchronized flapping of the wings. On the contrary, in the simple flexural and torsional modes a reaction force from the frame is needed to keep one end of the legs at rest, and the resulting clamping losses is thus dependent on the mechanical impedance of the sample holder and on its internal dissipation.

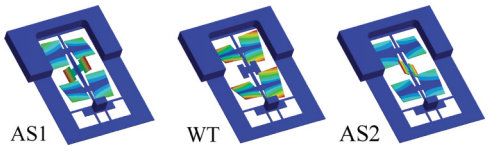

FIG. 3. (Color online) Maximum deformation of the QPO oscillator when vibrating in the high Q resonant modes; the vibration amplitude is shown in color code growing from blue to red (online only). Mode frequency of AS1, WT, AS2 mode at room temperature is, respectively, 3636.6, 3837.1, and 4057.3 Hz, the quality factor in vacuum are 1.15×10^5–0.78×10^5 and 1.1×10^5. We note that for these modes the motion of pad with the heater is negligible in this scale, as the legs remain at rest during the motion.

The resonator was obtained from a 300 ± 15-μm-thick, float-zone-refined, double-side-polished, $\langle 100 \rangle$-oriented, n-doped silicon wafer with a room temperature resistivity higher than 20 kΩ-cm. A silicon-oxide etch mask with the desired shape was first deposited on both sides of the wafer, then the geometry was obtained by wet etching in a Tetramethyl ammonium hydroxide water solution. This is an easy and cost-effective method for the fabrication of three-dimensional silicon microsensors, provided that specific efforts are devoted to control anisotropy effects and ensure strict dimensional tolerances for a proper functioning of the oscillator [19]. After the realization of the device, the masking oxide was etched in HF water solution and gold electrodes were evaporated on the wings. The electrodes on the QPO consist of a gold deposition of 50 nm over a 5-nm Cr adhesion layer. The gold layer covers the leg and the frame, while the head and neck were not coated in order to minimize the energy loss caused by metal films (see Fig. 2).

III. EXPERIMENTAL RESULTS

We performed measurements of the resonant frequency of the oscillator at different temperatures, in both equilibrium and nonequilibrium states. To determine the resonant frequency we excited mechanically the oscillators by feeding a sinusoidal voltage at frequency f_s close to the oscillator resonance (at f_o) to the piezoelectric actuator for the Al5056 oscillator and to an external electrode assembly placed in front of the electrodes evaporated on the wings (as in Ref. [19]) for the silicon oscillator; we connected the amplified oscillator output to a lock-in amplifier, which demodulated the oscillator signal at f_s. Hence, we removed the excitation and let the oscillator energy decay. From a linear fit of the drift of the phase change during the decay we inferred the difference $f_s - f_o$ and hence the oscillator resonance. From the decay of the oscillation amplitude, we also measured the quality factor of the resonance, which turned out to be, respectively, about 10^3 for the aluminum oscillator, 1.15×10^5–0.78×10^5 and 1.1×10^5 in vacuum and at room temperature, for the AS1-WT-AS2 resonant modes of the silicon oscillator. For the latter case, all other modes showed quality factors in the range 10^3–10^4. These values are in good agreement with the limit set by the thermoelastic dissipation in the device, evaluated by a finite element procedure [19,20].

A. Al5056 oscillator

The time constant for the energy decay of the Al5056 oscillator is about 0.2 s; thus, each measurement of the oscillator resonance lasted about 1 s. We collected 1467 measurements of the frequency of the first longitudinal mode during about 3 months; during this same period we measured the temperatures T_1 and T_2 with a sampling rate of 0.1 Hz. Part of the measurements were performed with the control loop of T_1 off, some with the control loop on, and some also with the thermal source on.

It is clear that when the temperature of the body is in fast drift, the temperature profile cannot be known to a good precision, since we only measure the temperature at the

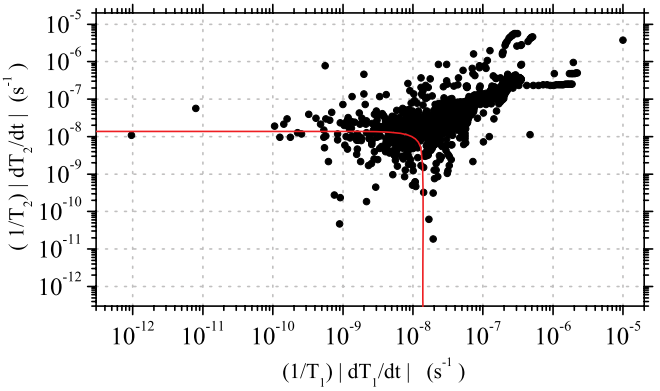

FIG. 4. (Color online) Plot of the absolute value of the normalized time derivative of the temperature T_1 and T_2 corresponding to each measurement of the resonant frequency of the oscillator. The solid line encloses the data, which are selected as steady-state ones.

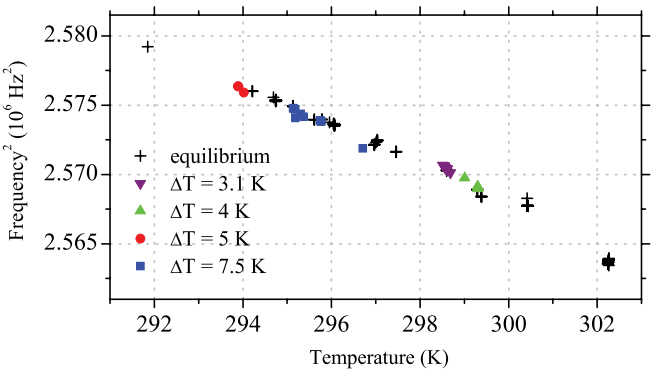

FIG. 5. (Color online) Plot of the square of the the oscillator resonant frequency vs. the average temperature for the equilibrium data (+) and nonequilibrium data [(purple) ▼ for $\Delta T = 3.1$ K, (green) ▲ for $\Delta T = 4$ K, (red) • for $\Delta T = 5$ K, (blue) ■ for $\Delta T = 7.5$ K] with constraints on time derivative.

extremes of the oscillator. However, due to the simplicity of the oscillator design, once the steady state is reached, it suffices to know T_1 and T_2 to infer the linear thermal profile along the rod given by the Fourier's law. Thus, in the steady states the temperature $T_{\rm avg} = (T_1 + T_2)/2$ corresponds to the average temperature of the rod, i.e., of the spring component of the oscillator, in a lumped model; in the same model the oscillator mass is at temperature T_2.

To identify the steady states, we computed the time derivative of T_1 and T_2 as the difference between two consecutive measurements divided by the sampling time. Since T_2 suffers from electronic noise, which appears as a jitter of ± 0.1 K, before computing its time derivative we passed the T_2 data through a smoothing procedure based on a triangular moving average performed on the time series.[1] Figure 4 shows the absolute value of the time derivative for each resonant frequency measurement, normalized by the measured temperature. The time derivatives of the two temperatures span several orders of magnitude, as expected, since we took measurements both when T_1 was controlled actively and when the system was in temperature drift.

To select the steady-state measurements we put an upper limit on the normalized total time derivative of the temperature $\sqrt{(\frac{1}{T_1}\frac{dT_1}{dt})^2 + (\frac{1}{T_2}\frac{dT_2}{dt})^2}$. We chose an upper limit of 1.4×10^{-8}/s, which corresponds to about 4 μK/s, thus rejecting 90% of the measurements and keeping only 145 measurements.

Figure 5 shows how the (square of the) oscillator resonance changes with the oscillator average temperature for the above selected steady-state measurements; on the same graph, we plot the data taken with zero temperature difference (i.e., thermal source off; equilibrium data) and those taken with a non-null-temperature difference (nonequilibrium data). The latter points fit well in the same distribution as the equilibrium data. We note that if we relax the criterion for choosing the steady-state measurements, the scatter of the measurements increases significantly; as discussed, the identification of the average temperature as $(T_1 + T_2)/2$ is not justified when the temperature of the metal piece is in drift.

The capacitor electric field exerts an attractive force between the plates, which lowers the resonance frequency with respect to the unbiased oscillator. We made sure that during the measurements there was no significative charge leakage. On the other hand, when a temperature difference is present across the oscillator, the latter expands with respect to the equilibrium state; thus, the gap is reduced and the electric field is correspondingly larger. The thermal coefficient of aluminum is $\alpha = 24 \times 10^{-6}$/K around room temperature; given a maximum difference of $\Delta T_{\rm max} = 9$ K and a length of the oscillator rod of $L = 0.1$ m, we estimate the rod to have expanded by $\delta L = 1/2\alpha L \Delta T_{\rm max} = 11\ \mu$m, the gap to have reached the extreme value of 33 μm (a 25% change) and correspondingly the electric field to have increased to 1.5×10^5 V/m. On the other hand, from independent measurements we estimated the effect of the electric field on the oscillator resonance to be about 7×10^{-8} Hz m/V and, thus, our measurements are affected by a maximal systematic error of 3×10^{-3} Hz, much less than the frequency change we observe in Fig. 5. Thus, we conclude that the impact of the thermal expansion on our measurements is negligible.

B. Silicon oscillator

In the case of the silicon resonator, the temperature of the sample holder was measured by a Cernox resistor and kept constant within 5 mK by a heater within a PID controller. The thermal difference was applied by a separate heater (20Ω resistor) fixed on to the pad prepared in the body of the device. The pad hosts also a PT100 thermometer to provide the measure of the applied temperature. The heater and the thermometer are both glued by a thermal conductive epoxy. We point out that, according to finite elements simulations, the

[1] Starting with the experimental data $T_{2,n}$, the filtered data $\tilde{T}_{2,n}$ was obtained by averaging over $2M + 1$ points using the formula ($M = 100$):

$$\tilde{T}_{2,n} = \frac{1}{(M+1)^2} \sum_{m=-M}^{M} (M + 1 - |m|)\, T_{2,n+m}. \qquad (1)$$

To simplify the notion, we use the symbol $T_{2,n}$ in the following instead of the correct one, $\tilde{T}_{2,n}$.

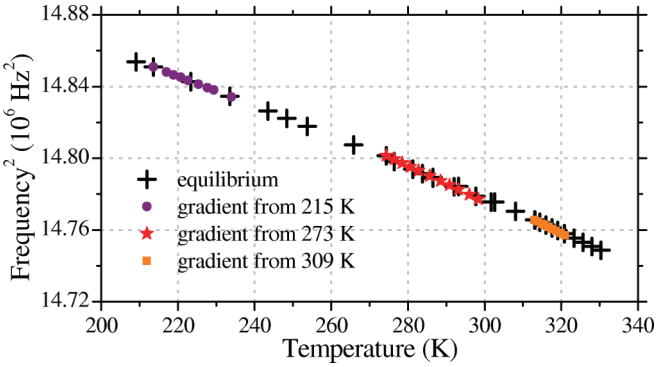

FIG. 6. (Color online) Plot of the square of the WT mode resonant frequency vs. the average temperature for the equilibrium and nonequilibrium data. The three curves in nonequilibrium were obtained by increasing the temperature of one side of the resonator, while the other side is kept fixed at, respectively, 215 (purple •), 273 (red ★), and 309 K (orange ■). In these curves, each point is plotted in correspondence of the average temperature of the resonator $(T_1 + T_2)/2$. The maximum applied temperature difference was about 50 K (25 K for the data set starting at 309 K) and the stability of the temperature of both sides during the measurement was better than ±5 mK. Modes AS1 and AS2 have a similar behavior.

mass of the attached components has negligible effects on the frequencies and the quality factors of the modes under study.

When the heater was powered, the temperature of the pad remained constant within 5 mK after a transient time of about 15 min. We point out that the thermal control of the silicon oscillator is much less demanding than that of the aluminum one. In fact, in the former case the mass is much lower and the thermal response time of the system is about two orders of magnitude faster, allowing an higher closed-loop gain of the thermal control without the risk of auto-oscillations. The residual temperature drift was about 5 μK/s. As shown in Fig. 6, we first measured the temperature dependence of (square of) the resonant frequency in equilibrium over a temperature range between 215 and 330 K; then the temperature of the sample holder was kept fixed at 215, 273, and 309 K and the heater on the device was powered. The resonant frequency was measured for thermal differences up to 50 K. For the data set starting from 309 K we limited the thermal difference to 25 K to avoid the overheating of the epoxy glue used to fix the thermometer and the heater onto the pad. As reported in Fig. 6 for one of the resonant modes under observation, the measured frequency, when a temperature difference $\Delta T = T_2 - T_1$ is applied, approaches very well the frequency measured in equilibrium at the average temperature $(T_1 + T_2)/2$.

IV. NUMERICAL MODEL

In order to investigate the statistical mechanical properties of our oscillators in nonequilibrium steady states, we have developed a numerical model of a solid bar. We keep the model as simple as possible and consider the case of a linear chain of nonharmonic oscillators; we aim to explain in a general fashion, rather than quantitatively, its elastic response to nonequilibrium conditions, namely, as they compare to equilibrium ones. The model considers N particles, constrained to move in one dimension, each interacting with a fixed number of neighboring particles via some interaction potential $W(r)$. The boundary conditions replicate different phenomenological setups, like a rod with fixed ends, or a rod with one fixed and one free end, and so on.

In spite of its simplicity, we have already proved [15] that with an informed choice of the interparticle potential, our model is able to reproduce main thermomechanical traits of most solids, namely the thermal expansion and the variation of the elasticity modulus with temperature. The only hypotheses we required to be satisfied by the model is that at equilibrium the probability for a microscopic configuration to be visited is well approximated by a canonical distribution. Here we extend our investigation of the model to nonequilibrium steady states; thus, we add a second requirement, namely that out of equilibrium, such distribution becomes modified in such a way that it nonetheless satisfies some notion of local equilibrium, to be specified later.

To compare with the experimental results, we consider a linear chain with particles moving along the x coordinate, with the left edge that is fixed and a force F that is applied to the right edge, pointing toward the left. The average length $L = L(F)$ is a function of such force, and from its rate of change in the limit of vanishing F we extract the elastic response of the chain. Thus, we define the elastic coefficient E to be

$$E = -\frac{L(0)}{\frac{\partial L}{\partial F}\Big|_{F=0}}. \tag{2}$$

If we are given the probability distribution $p(\mathcal{L},F)$ that a microscopic configuration be found with $(\mathcal{L},F)$ in the (length,force)-space, then it follows that

$$L(F) = \int_0^\infty \mathcal{L}\, p(\mathcal{L},F)\, \mathrm{d}\mathcal{L}. \tag{3}$$

Each choice of the interaction potential $W(r)$ generates its own probability distribution $p(\mathcal{L},F)$, which is implicitly a function of N, the number of particles. At equilibrium, $p(\mathcal{L},F)$ is also a function of the temperature T, while when the temperature is not uniform (like when a difference is generated between the two ends), its dependence on the temperature profile may be nontrivial. In the following, we discuss briefly the theoretical results regarding the equilibrium case derived in Ref. [15] so as to extend them to the non-equilibrium case in Sec. IV B. Then, in Sec. IV C we consider explicit calculations for the modulus of elasticity. Finally, in Sec. IV D we compare the theoretical results with numerical simulations.

A. The equilibrium case

In this case, the form assumed by $p(\mathcal{L},F)$ is [15]

$$p(\mathcal{L},F) = \frac{e^{-\frac{F\mathcal{L}}{k_B T}} \int_0^{\mathcal{L}} dr_1 \int_{r_1}^{\mathcal{L}} dr_2 \ldots \int_{r_{N-1}}^{\mathcal{L}} dr_N\, G(r_1, r_2, \ldots, \mathcal{L})}{\int_0^\infty d\mathcal{L}\, e^{-\frac{F\mathcal{L}}{k_B T}} \int_0^{\mathcal{L}} dr_1 \int_{r_1}^{\mathcal{L}} dr_2 \ldots \int_{r_{N-1}}^{\mathcal{L}} dr_N\, G(r_1, r_2, \ldots, \mathcal{L})}, \tag{4}$$

where

$$G(r_1, r_2, \ldots, \mathcal{L}) = \psi(r_1)\psi(r_2 - r_1)\ldots\psi(\mathcal{L} - r_N), \quad (5)$$

with $\psi(r)$ the Boltzmann factors

$$\psi(r) = e^{-\frac{W(r)}{k_B T}}, \quad (6)$$

where the kinetic terms in the numerator and the denominator cancel each other out.

The useful quantity in the calculation is the integral appearing in the denominator of Eq. (4), call it $\mathcal{Z} = \mathcal{Z}(F,T,N)$, which can be recognized as a Laplace transform of a chained convolution product, thus expressible as

$$\mathcal{Z} = [j_0(F;T)]^N; \quad j_k(F;T) = \int_0^\infty r^k e^{-\frac{Fr}{k_B T}}\psi(r)\,dr. \quad (7)$$

This explicit expression of $\mathcal{Z}$ is useful if we revert to Eq. (3) and recognize that

$$L(F) = -\frac{k_B T}{\mathcal{Z}}\frac{\partial \mathcal{Z}}{\partial F} = \frac{N j_1(F;T)}{j_0(F;T)}. \quad (8)$$

We note that for phenomenological interaction potentials, the low dimensionality of the system causes a few pathologies, as in the case of $L(0)$, the equilibrium length when no force is applied, which is defined in Eq. (8) via diverging integrals. To avoid these problems we constrain our system to be bound by some recoil force, which prevents the particles to separate more than a certain distance R (much larger than the average interparticle distance). Formally, all throughout we replace $j_k(F=0;T)$ with $J_k(T)^{(R)} = \int_0^R r^k\psi(r)\,dr$, now convergent. Provided R is large enough, the rationale for this is that, in the low-temperature ordered state, large interparticle separations are very rare and the measure is dominated by separations which are never too large. This in turn implies that $J_k(T)^{(R)}$ is only weakly dependent on R and for simplicity, in the following, we shall omit the R-dependence.

With this in mind, we can now give a meaning to the definition of E in Eq. (2), from Eq. (8), now reading

$$E = -\frac{N J_1(T)}{J_0(T)}\frac{J_0(T)^2}{N[J_0(T)j_1'(F;T)|_{F=0} - J_1(T)j_0'(F;T)|_{F=0}]} = \frac{k_B T J_0(T)J_1(T)}{J_0(T)J_2(T) - J_1(T)^2}. \quad (9)$$

B. The nonequilibrium case

In order to extend our results out of equilibrium we must implement some reformulation of $p(\mathcal{L},F)$. Rather than developing a rigorous treatment, here we adopt a modified expression under the strong assumption that the distribution is locally canonical (when the marginal distribution of the particles' coordinates is considered) down to the particle-by-particle scenario. This is somewhat consistent with the observation that in these models a local version of the virial theorem typically holds (as we have also verified for our models). Thus, we make the replacement

$$\psi(r_i - r_{i-1}) \to \psi_i(r_i - r_{i-1}) = e^{-\frac{W(r_i - r_{i-1})}{k_B T_i}}, \quad (10)$$

with T_i the "local" temperature along the chain. This leads to

$$\mathcal{Z} = \prod_{i=1}^N j_0(F;T_i), \quad (11)$$

and, therefore, to

$$L(F) = -\frac{k_B T}{\mathcal{Z}}\frac{\partial \mathcal{Z}}{\partial F} = \sum_{i=1}^N \frac{j_1(F;T_i)}{j_0(F;T_i)} = \frac{1}{N}\sum_{i=1}^N L(F;T_i) \quad (12)$$

$$\left.\frac{\partial L}{\partial F}\right|_{F=0} = \frac{1}{N}\sum_{i=1}^N \left.\frac{\partial L(F;T_i)}{\partial F}\right|_{F=0} = -\frac{1}{N}\sum_{i=1}^N \frac{L(0;T_i)}{E_{T_i}}, \quad (13)$$

where $L(F;T_i)$ and E_{T_i} are, respectively, the average length, when a force F is applied, and the modulus of elasticity that the system would have if the entire chain were at equilibrium at the temperature T_i. From the general definition of E [Eq. (2)] and from Eqs. (12) and (13), we have

$$E = \frac{\sum_{i=1}^N L(0;T_i)}{\sum_{i=1}^N \frac{L(0;T_i)}{E_{T_i}}}. \quad (14)$$

It is more instructive to consider E^{-1}, which is seen to be the weighted average of its values along the chain, with weights $L(0;T_i)$, i.e.,

$$E^{-1} = \frac{\sum_{i=1}^N E_{T_i}^{-1} L(0;T_i)}{\sum_{i=1}^N L(0;T_i)} = \frac{1}{N\,L(0)}\sum_{i=1}^N E_{T_i}^{-1} L(0;T_i). \quad (15)$$

C. Physical approximations

In principle, Eqs. (14) and (15) can imply nontrivial results for E. Nevertheless, the situation is not as severe as it looks at a first glance, if we implement physical assumptions consistent with the experimental conditions. Therefore, we assume that the equilibrium elastic constant E varies linearly with T [4], throughout the range of temperatures of interest. We define T_1 and T_2 ($T_1 < T_2$), the temperatures at the left and right extremes of the chain, respectively. Equally consistently with the real situation, we restrict our analysis to the case $\frac{1}{L}\frac{dL}{dT} \ll \frac{1}{E}\frac{dE}{dT}$ inside the $[T_1,T_2]$ range. Accordingly, we always consider $L(0)$ to be almost constant and well approximated by the average length of the chain if it were at equilibrium at the average temperature $\overline{T} = \frac{T_1+T_2}{2}$, which is $L(0;\overline{T})$. In Eq. (2), this corresponds to the case in which the change of $\frac{\partial L}{\partial F}|_{F=0}$ carries most of the change of E with temperature. Under the assumed linearity of E for $T \in [T_1,T_2]$, E_{T_i} decreases linearly with T_i, i.e.; if we pass to the continuum limit,

$$E(T) = \alpha - \beta\,T; \quad \alpha = \frac{E_{T_1}T_2 - E_{T_2}T_1}{\Delta T}, \quad \beta = \frac{\Delta E}{\Delta T}, \quad (16)$$

with $\Delta E = E_1 - E_2$ and $\Delta T = T_2 - T_1$. Then, if $L(T)$ is slowly varying,

$$E^{-1} \simeq \frac{\int_{T_1}^{T_2} E(T)^{-1} L(T) dT}{\int_{T_1}^{T_2} L(T) dT} = \frac{1}{\Delta T} \int_{T_1}^{T_2} \frac{dT}{\alpha - \beta T} = \frac{1}{\Delta E} \log \frac{E_1}{E_2}. \quad (17)$$

We define $\overline{E} = E_{\overline{T}}$, the modulus of elasticity one would have with the chain at equilibrium at the average temperature $\overline{T}$ (i.e., if the entire chain were at $\overline{T}$). Equation (17) implies a general inequality $E \leqslant \overline{E} \equiv E_{\overline{T}}$. When the relative difference is small, i.e., $\Delta E \ll \overline{E}$, Eq. (17) further implies $E \simeq \overline{E}$, so the modulus of elasticity of the chain with a standing temperature difference is approximately equal to the modulus of elasticity of a chain that is at equilibrium at the average temperature. This is precisely what we see in the experiments. Adding the next correction in $\frac{\Delta E}{\overline{E}}$ into Eq. (17) is also straightforward, leading to

$$E \cong \overline{E} \left[1 - \frac{1}{12} \left(\frac{\Delta E}{\overline{E}} \right)^2 \right], \quad (18)$$

and, therefore, the first correction is quadratic in $\Delta E / \overline{E}$.

The result relating E to $\overline{E}$ is sufficiently robust to also hold, at the lowest order, if $L(T)$ is not a constant but linear in T, i.e., if $L(T) \simeq \gamma + \delta T$ (here we omit the proof).

D. Simulations

We have tested the theoretical results against computer molecular dynamics simulations. We considered Lennard-Jones (LJ) potential for the interparticle interaction $W(r)$:

$$W(r) = \epsilon \left[\left(\frac{r_0}{r} \right)^{12} - 2 \left(\frac{r_0}{r} \right)^{6} \right]. \quad (19)$$

The canonical ensemble, at equilibrium, is attained with the implementation of Nosé Hoover thermostats at the boundaries [23]. Out of equilibrium, the thermostats are set to two different target temperatures. The temperature at each point along the chain is identified with the average kinetic temperature of each individual particle. A known preliminary problem for these models with first-neighbor interaction is that the temperature profile, i.e., the profile of the average kinetic temperatures, is not linear but somewhat *S*-shaped [21]. As an example, Fig. 7 shows the typical temperature profile that we obtain with our simple model.

To circumvent this limitation, we developed a refined model with first- and second-neighbors interactions. To preserve the stability of the "crystal" structure, the range of the interaction between two particles which are second-next neighbors is tuned at exactly twice the range of the interaction between two particles which are first-neighbors. Therefore, in the bulk, each particle has direct interaction with four rather than two neighbors. The depths of the well were chosen to be the same, which means that (because of the modified range) the strength of the bonds between second-neighbors is approximately one quarter of that between first neighbors. Nevertheless, the bonds are reinforced and thus the elastic recoil constants are. More explicitly, if Eq. (19) represents the interaction between

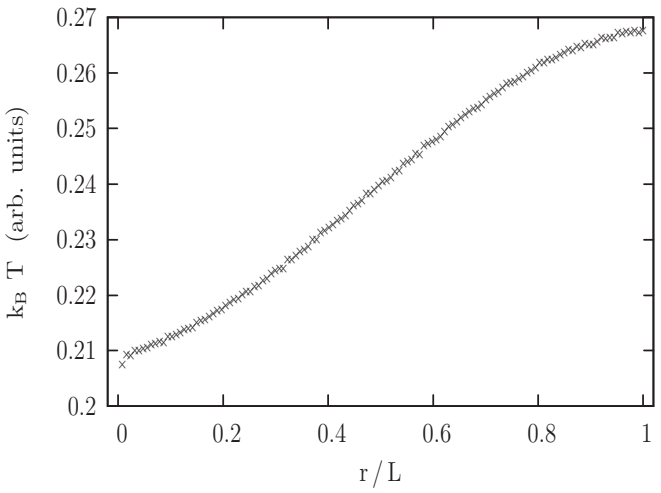

FIG. 7. Typical temperature profile, as a function of the reduced coordinate r/L, of a linear chain with only nearest-neighbor interactions.

two particles which are first neighbors, then between second neighbors we would have,

$$W(r) = \epsilon \left[\left(\frac{2r_0}{r} \right)^{12} - 2 \left(\frac{2r_0}{r} \right)^{6} \right]. \quad (20)$$

In this model we have four Nosè-Hoover thermostats, each acting individually on one specific particle to guarantee that its average kinetic energy is the one set as target temperature. The four thermostatted particles are: the two leftmost particles, at T_1; the two right-most particles, at T_2. At the two extremes, two additional virtual particles are added to represent the walls, i.e., the fixed boundaries. The length separating them is such that the average force exerted by the whole chain on the walls is approximately zero.

The result for the new temperature profile can be seen in Fig. 8, for three choices of temperatures and, correspondingly, two choices of relative temperature differences. The temperature profile is now almost linear in the bulk, in the range between a temperature which is slightly higher than T_1 and one which is slightly lower than T_2. Indeed, and unpredicted, we can see a slight temperature jump at the points of contact of the chain with the thermostatted boundaries, a sort of "contact resistance," which has been usually found in one-dimensional systems, cf. [22]. Despite this effect, which slightly limits our capacity to control the temperature gradient exactly, for all other practical purposes we are well within the theoretical requirements discussed in the previous sections.

To calculate the elastic coefficient E from simulations, we have used the same method as the one described in Ref. [15]. For each temperature, and temperature difference, the simulations are run with the two ends clamped. After some appropriate averaging, the total distance between the two ends is routinely varied, and in each instance the average force exerted on the clamped particle by the neighboring ones is calculated. There will be a distance, which previously we have called $L(0;T)$, in correspondence of which such average force is null. In the proximity of $L(0;T)$, the same force will be proportional to $\frac{\Delta L}{L}$. The proportionality constant is, therefore, E.

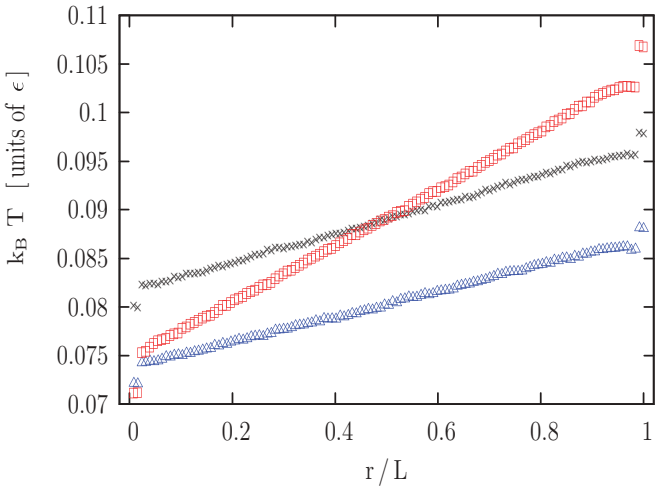

FIG. 8. (Color online) Temperature profile, as a function of the reduced coordinate r/L, of a linear chain with only nearest and second-nearest neighbor LJ interactions. The temperature is presented in units of the LJ energy scale ϵ. If we take as a reference the (black) $\times$ points, referring to a relative difference $\Delta T_\times/\overline{T_\times} = 0.2$, and the corresponding $\overline{T_\times}$ average temperature, then the (blue) $\triangle$ points refer to $\overline{T} = 0.9\,\overline{T_\times}$ and $\Delta T/\overline{T} = 0.2$, and the (red) $\square$ points refer to $\overline{T} = \overline{T_\times}$ and $\Delta T/\overline{T} = 0.4$.

In Fig. 9 we present results for the elasticity modulus E, in function of T for the equilibrium case, and in function of $\overline{T} = (T_1 + T_2)/2$ for the nonequilibrium cases. The relative differences are such that $\Delta T/\overline{T} = 0.2$ or $\Delta T/\overline{T} = 0.4$. $N = 128$ for all cases but one among the two in which $\Delta T/\overline{T} = 0.4$, in which case $N = 256$. When $\Delta T/\overline{T} = 0.2$, our results are entirely consistent with the theoretical predictions of the previous sections (despite the fact that now the interaction includes second-neighbors bonds, which was not part of the derivation). That is, one would not be able to distinguish

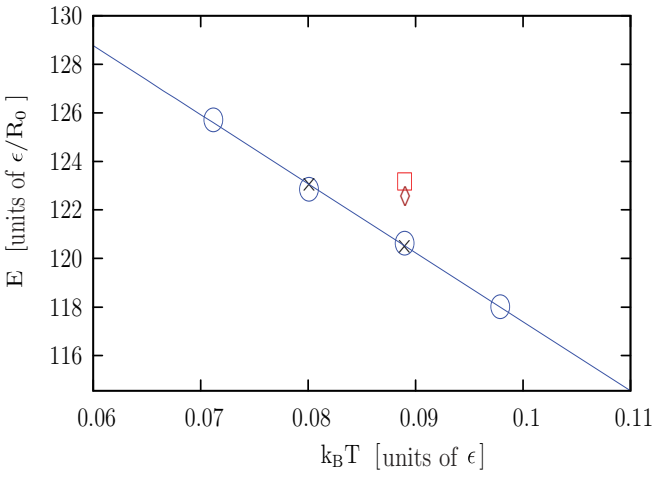

FIG. 9. (Color online) The modulus of elasticity E as a function of the temperature, i.e., equilibrium temperature for equilibrium simulations with $N = 128$ [the (blue) $\bigcirc$ points and the (blue) linear fit]; average temperature $\overline{T}$ for nonequilibrium simulations. The (black) $\times$ points are for the case $N = 128$ and $\Delta T/\overline{T} = 0.2$. The (red) $\square$ point is for $N = 128$ and $\Delta T/\overline{T} = 0.4$. The (wine) $\diamondsuit$ point is for $N = 256$ and $\Delta T/\overline{T} = 0.4$.

between a chain with a temperature difference actively sustained between the two extremes and one which is at equilibrium at the temperature $\overline{T}$. On the other hand, the situation changes when $\Delta T/\overline{T} = 0.4$. In this case, E is noticeably larger than expected. For the reasons explained in the preceding sections, this difference cannot be explained away invoking some correction originating from the increased magnitude of $\Delta E/\overline{E}$, as this would be smaller, as well as pointing toward smaller rather than larger values of E. For this particular case, we have also used $N = 256$, which maintains the same particle-to-particle temperature difference as the one established when $\Delta T/\overline{T} = 0.2$ and $N = 128$, but this has not resolved the anomaly. We argue that this anomaly might be model-related. For example, the hypothesis that the system is locally canonical, or effectively equivalent to a locally canonical system, is not justified when the relative difference, hence the dissipation, is too large. It is also known that many thermostats used in molecular dynamics simulations fail to behave in a physically sound manner when $\Delta T/\overline{T}$ or, more generally, the dissipation exceeds certain limits [24–26], and this could have nontrivial repercussions on the elastic behavior of the chain. By converse, the case $\Delta T/\overline{T} = 0.2$ shows impressive agreement with both the theoretical predictions and the elastic properties described by the experiments.

V. CONCLUSIONS

We have demonstrated with both experimental and numerical investigations that, as far as the elastic behavior is concerned, a solid-body subject to steady-state thermal differences is equivalent to the same body in equilibrium at the average temperature. Here, by average temperature we mean either the volume averaged temperature of a body which is symmetric with respect to an axis orthogonal to the thermal gradient (as in Secs. III B and IV D) or the volume averaged temperature of the elastic component of the body in a lumped scheme (as in Sec. III A). The symmetry properties of our experimental setup make it easy to measure such average temperature. In general, this is not the case; indeed, the resonant frequency of an acoustic mode can be used to infer its average temperature. This finding is true both in the case of a metal and of a semiconductor. We have also developed a theoretical explanation of the above findings, under the assumption of local equilibrium. This suggests that, insofar as the elastic properties are considered, there is a consistency between the temperature that a thermometer measures and the notion of local-equilibrium temperature. Or, differently said, it shows that the purely elastic response is unaffected by the magnitude of the standing heat flux. On other grounds, whether this is a general fact for nonequilibrium observables remains an open question in the thermodynamics community (see Ref. [27] and references therein). Further, we have shown that violations of Fourier's Law in models consisting of one-dimensional chains of anharmonic oscillators can be overcome by taking into account longer-range interactions. We have also observed a discrepancy on the Young's modulus with the numerical experiment, but this only emerges at a level of relative thermal differences (40%) much larger than the relative thermal differences set in the experimental work ($\lesssim$15%).

ACKNOWLEDGMENTS

The research leading to these results has received funding from the European Research Council under the European Community's Seventh Framework Programme (FP7/2007-2013)/ERC Grant No. 202680.

[1] A. P. Boresi and R. J. Schmidt, *Advanced Mechanics of Materials* (Wiley, New York, 2002).
[2] K. A. Topp and D. G. Cahill, Z. Phys. B **101**, 235 (1996).
[3] Pablo Esquinazi (Editor), *Tunneling Systems in Amorphus and Crystalline Solids* (Springer, Berlin, 1998).
[4] J. B. Wachtman Jr, W. E. Tefft, D. G. Lam Jr, and C. S. Apstein, Phys. Rev. **122**, 1754 (1961).
[5] Y. P. Varshni, Phys. Rev. B **2**, 3952 (1970).
[6] G. Fauconneau and R. D. Marangoni, Int. J. Mech. Sci. **12**, 113 (1970).
[7] J. S. Tomar and A. K. Gupt, J. Sound Vib. **98**, 257 (1985).
[8] C. K. Hruska and H. H.-Y Hui, IEEE Trans. Sonics Ultrason. **SU-32**, 604 (1985).
[9] L. Conti, M. Bonaldi, and L. Rondoni, Cl. Quant. Grav. **27**, 084032 (2010).
[10] R. Kubo, Rep. Prog. Phys. **29**, 255 (1966).
[11] U. Marini, Bettolo Marconi, A. Puglisi, L. Rondoni, and A. Vulpiani, Phys. Rep. **461**, 111 (2008).
[12] O. D. Aguiar, Res. Astr. Astrophys. **11**, 1 (2011).
[13] R. Ghodssi and P. Lin (Editors), *MEMS Materials and Processes Handbook* (Springer, Berlin, 2011).
[14] [http://www.et-gw.eu/].
[15] P. De Gregorio, L. Rondoni, M. Bonaldi, and L. Conti, Phys. Rev. B **84**, 224103 (2011).
[16] M. Saraceni, M. Bonaldi, L. Castellani, L. Conti, A. B. Gounda, S. Longo, and M. Pegoraro, Rev. Sci. Instrum. **81**, 035115 (2010).
[17] S. Longo, L. Cecchinato, M. Rampazzo, M. Bonaldi, A. Beghi, and L. Conti, Eur. Phys. J. Appl. Phys. **57**, 21001 (2012).
[18] C. L. Spiel, R. O. Pohl, and A. T. Zehnder, Rev. Sci. Instrum. **72**, 1482 (2001).
[19] A. Borrielli, M. Bonaldi, E. Serra, A. Bagolini, and L. Conti, J. Micromech. Microeng. **21**, 065019 (2011).
[20] E. Serra and M. Bonaldi, Int. Jour. Num. Meth. Eng. **78**, 671 (2009).
[21] S. Lepri, R. Livi, and A. Politi, Phys. Rep. **377**, 1 (2003).
[22] C. Giberti and L. Rondoni, Phys. Rev. E **83**, 041115 (2011).
[23] D. C. Rapaport, *The Art of Molecular Dynamics Simulations*, 2nd ed. (Cambridge University Press, Cambridge, 2004).
[24] D. J. Evans and G. P. Morriss, in *Statistical Mechanics of Nonequilibrium Liquids*, 2nd Edition (Cambridge University Press, Cambridge, 2008).
[25] C. Mejia-Monasterio and L. Rondoni, J. Stat. Phys. **133**, 617 (2008).
[26] O. G. Jepps and L. Rondoni, J. Phys. A **43**, 133001 (2010).
[27] J. Casas-Vazquez and D. Jou, Rep. Prog. Phys. **66**, 1937 (2003); V. A. Cimmelli, J. Non-Equilib. Thermodynam. **34**, 299 (2009).